Available online at www.sciencedirect.com

ScienceDirect

IFAC PapersOnline CONFERENCE PAPER ARCHIVE

IFAC PapersOnLine 59-1 (2025) 151–156

A Benchmark Model for Model Order Reduction: Large-scale Wind Farms

Hanqing Zhang * **Zilong Gong** * **Adrià Junyent-Ferré** * **Giordano Scarciotti** *

* *Electrical and Electronic Engineering Department, Imperial College London, London, UK (e-mail: hanqing.zhang21@imperial.ac.uk, zilong.gong18@imperial.ac.uk, adria.junyent-ferre@imperial.ac.uk, g.scarciotti@imperial.ac.uk)*

Abstract: A large-scale wind farm model is presented as a benchmark model for various model order reduction (MOR) methods. Firstly, the detailed mathematical description of a wind turbine generator is provided, including the aerodynamic and mechanical sub-blocks of the wind turbine, the electrical sub-block of the generator, and the associated controllers. Based on the wind turbine generator model, a large-scale wind farm model is created whose dimension can be easily changed to test MOR methods on different scales. Finally, the wind farm model is utilised as a benchmark model to show the performance of a nonlinear MOR method and a linear MOR method.

Copyright © 2025 The Authors. This is an open access article under the CC BY-NC-ND license (https://creativecommons.org/licenses/by-nc-nd/4.0/)

Keywords: Wind farm, model reduction, benchmark model, power system, nonlinear system.

1. INTRODUCTION

The simulation and analysis of large-scale systems, which are commonly represented by numerous ordinary differential equations and thus are of high order, tend to be computationally expensive and time-consuming. This problem exists in many practical cases, *e.g.*, power systems, see Scarciotti (2016), weather forecasting and differential systems arising from finite element analysis, see Antoulas (2005). To reduce the computational resources needed for the analysis of large-scale systems, MOR methods have been extensively investigated Antoulas (2005). Using MOR techniques, one can obtain a reduced-order model of the large-scale system which, being described by fewer ordinary differential equations, needs less time and fewer computational resources to analyse and simulate.

As more and more different types of MOR methods have been developed, see *e.g.*, Kawano and Scherpen (2021); Scarciotti and Astolfi (2024); Janssen et al. (2024), benchmark models are highly demanded to test the behaviour and efficacy of these methods. To this end, the website The MORwiki Community (N.D.) collects various benchmark models of large-scale systems, rendering it convenient to test different MOR methods on different types of systems. The MORwiki community mainly provides benchmark models for linear MOR, which is attributed to the fact that most MOR methods have been developed for linear cases in recent decades. However, as more and more nonlinear MOR methods have been proposed in the past decade, see *e.g.*, Besselink et al. (2014); Fujimoto and Scherpen (2010); Simard and Astolfi (2021); Astolfi (2010); Bond and Daniel (2007), benchmark models for nonlinear MOR are increasingly required.

In this paper, we present a large-scale wind farm model as a benchmark model for MOR. This model has recently been developed in the context of model reduction of large-scale power systems obtained from the interconnection of renewable and classical generators Gong et al. (2024) and is now described here in full detail. The wind farm model is nonlinear and thus is suitable for testing nonlinear MOR methods. Additionally, the wind farm can also be used to test linear MOR methods after linearisation. This is reasonable because the performance of power systems around an operating point is of great interest, see *e.g.* Ali et al. (2018). While benchmark models of classical (synchronous) power systems are available in the literature, see *e.g.* Rafiq and Bazaz (2023), as far as the authors know our contribution is the first instance of a detailed benchmark model of a large-scale wind farm (which is of increasing interest in the power system community).

The rest of the paper is organized as follows. Section 2 provides the detailed mathematical model of a single wind turbine generator, including its aerodynamic, mechanical, and electrical parts, as well as the associated controllers. Based on the wind turbine generator model, Section 3 schematically presents a large-scale wind farm model and discusses its possible variations. Finally, the use of the benchmark wind farm model is illustrated by applying multiple MOR techniques in Section 4.

2. WIND TURBINE GENERATOR MODEL

A wind turbine generator commonly consists of mechanical and electrical modules. The mechanical module extracts mechanical energy from wind through blades, while the electrical module converts the supplied mechanical energy to the electrical energy by a rotor. In the following subsections, we describe the model of the wind turbine generator as originally developed in Junyent Ferré (2011), while turbine misalignment (yaw errors) is neglected, meaning that

2405-8963 Copyright © 2025 The Authors. This is an open access article under the CC BY-NC-ND license.
Peer review under responsibility of International Federation of Automatic Control.
10.1016/j.ifacol.2025.03.027

the considered wind speed in this section is the wind speed component perpendicular to the wind turbine blades.

2.1 Wind Turbine Mechanism

Wind turbine aerodynamics. A wind turbine extracts the kinetic power of the wind with a power coefficient C_p. The extracted power can be expressed by the kinetic power of the wind multiplied by the power coefficient C_p, namely

$$P_t = C_p P_w = C_p \frac{1}{2}\rho A v_w^3, \tag{1}$$

where P_t is the power extracted by the wind turbine, P_w is the kinetic power of the wind, ρ is the air density, A is the wind turbine swept area, and v_w [1] is the vertical component of the average wind speed. The power coefficient C_p is usually determined by Heier (2014)

$$\begin{aligned} &C_p(\Lambda,\beta) = c_1(c_2\frac{1}{\Lambda} - c_3\beta - c_4\beta^{c_5} - c_6)e^{-c_7\frac{1}{\Lambda}}, \\ &\frac{1}{\Lambda} = \frac{1}{\lambda + c_8\beta} - \frac{c_9}{1+\beta^3}, \quad \lambda = \frac{\omega_t R}{v_w}, \end{aligned} \tag{2}$$

where β is the blade pitch angle, ω_t is the angular speed of the turbine, R is the turbine radius and λ is the so-called tip speed ratio. The symbols $c_1, \ldots, c_9$ denote the characteristic parameters of the wind turbine which are obtained by testing a real wind turbine and should have been provided by the wind turbine manufacturer.

Dividing (1) by ω_t, we obtain the wind turbine torque

$$\Gamma_t = \frac{1}{2} C_p \rho A v_w^3 \frac{1}{\omega_t}. \tag{3}$$

The wind turbine torque Γ_t is utilised to control the wind turbine speed in the next section.

Drivetrain dynamics. The drivetrain is a mechanical system which connects the wind turbine to the rotor of the generator through the turbine shaft, the gearbox, and the rotor shaft. Herein, we simply consider the one-mass model [2] of the drivetrain which is expressed by

$$\begin{aligned} \frac{d}{dt}\omega_t &= \frac{1}{(I_m\nu^2 + I_t)}\Gamma_t - \frac{\nu}{(I_m\nu^2 + I_t)}\Gamma_m \\ &= \frac{1}{I_a}(\Gamma_t - \nu\Gamma_m), \end{aligned} \tag{4}$$

where ν is the gear ratio, Γ_m is the generator torque, I_m is the inertia of the rotor and gearbox, I_t is the inertia of the turbine, and $I_a \triangleq (I_m\nu^2 + I_t)$ is the aggregated inertia of the one-mass drivetrain.

Pitch angle control. To maximize the extracted power (1), the power coefficient C_p needs to be maximized with respect to β and λ, respectively. The pitch angle control aims to maximize C_p with respect to β by adjusting the pitch angle to a desired value using a pitch actuator. The pitch actuator is typically described as a first-order system

$$\frac{d}{dt}\beta = \frac{1}{\tau}(\beta^* - \beta), \tag{5}$$

whose associated transfer function is

$$\beta(s) = \frac{1}{\tau s + 1}\beta^*(s), \tag{6}$$

where τ is the time constant corresponding to the pitch actuator and β^* is the reference value for the pitch angle.

To achieve the pitch angle control, we apply a PI controller as follows

$$\beta^*(s) = \frac{K_p s + K_i}{s}(\omega_m(s) - \omega_{mn}(s)), \tag{7}$$

where $\omega_m = \nu\omega_t$ is the mechanical angular speed, ω_{mn} is the nominal mechanical angular speed, and K_p and K_i are the proportional and integral gains of the PI controller, respectively.

Speed control of the wind turbine. The speed control of the wind turbine aims to maximize C_p with respect to λ. We can see from (2) that λ depends on both the angular speed of the turbine ω_t and the average wind speed v_w. Based on this observation, to keep λ at the optimal value [3], the turbine angular speed ω_t should be controlled at different values as the wind speed changes. Since proper measurement of wind speed is practically unavailable, we consider here the *constant tip speed ratio control* method Leidhold et al. (2002), a widely used maximum power point tracking (MPPT) strategy, which is able to control ω_t to reach the desired value without the knowledge of the wind speed. Then we have

$$\begin{aligned} K_{C_p} &= \frac{1}{2}\rho A R^3 \frac{c_1(c_2 + c_6c_7)^3 e^{-\frac{c_2 + c_6c_7}{c_2}}}{c_2^2 c_7^4}, \\ \Gamma_m^* &= \Gamma_m^{opt} = \frac{1}{\nu} K_{C_p}\omega_t^2, \end{aligned} \tag{8}$$

where Γ_m^{opt} is the optimal generator torque and Γ_m^* is the generator torque reference value, which the generator control should achieve. It is noted from (4) that controls are imposed on ω_t implicitly through the control of Γ_m.

2.2 Generator Dynamics

We consider the permanent magnet synchronous generator (PMSG), a widespread type of generator for wind turbines. The main advantage of the PMSG is that the generator is completely isolated from the grid and therefore *is not* influenced by any grid-side disturbance.

Stator current dynamics. The dynamical equation of the PMSG is given by

$$v_s^{abc} = r_s i_s^{abc} + \frac{d}{dt}\lambda_s^{abc}, \tag{9}$$

where r_s is the single-phase resistance of the stator windings, v_s^{abc} is the three-phase stator voltage vector [4], i_s^{abc} is the three-phase stator current vector, and λ_s^{abc} is the three-phase stator flux linkage vector.

[1] In this paper, v_w is considered between the cut-in and cut-out wind speeds, meaning that the start-up and shut-down modes of the wind turbine are not of interest. This is because the start-up or shut-down mode usually introduces hard nonlinearity to the wind turbine model, to which case some of the existing model reduction techniques may not be applicable.

[2] The one-mass model neglects the damping ratio and the stiffness of the shafts which connect the turbine to the rotor, assuming the turbine, the gearbox, the shafts, and the rotor are lumped together.

[3] The optimal value of λ refers to the value at which the power coefficient C_p is maximazed with respect to λ.

[4] Namely, $v_s^{abc} = \begin{bmatrix} v_{sa} & v_{sb} & v_{sc} \end{bmatrix}^\top$, and other variables in this paper with superscripts *abc* or *qd* are defined in the same way.

In particular, the stator flux linkage vector λ_s^{abc} can be expressed as

$$\lambda_s^{abc} = (L_1 + L_2(\theta_r))i_s^{abc} + \lambda_m \begin{bmatrix} \sin(\theta_r) \\ \sin(\theta_r - \frac{2\pi}{3}) \\ \sin(\theta_r + \frac{2\pi}{3}) \end{bmatrix}, \quad (10)$$

where θ_r denotes the rotor electric angle and λ_m denotes the flux linkage per rotating speed unit. The symbols L_1 and $L_2(\theta_r)$, as given in (11), represent the inductance component that is independent of θ_r and the inductance component that is dependent on θ_r, respectively.

$$\begin{aligned} L_1 &= \begin{bmatrix} L_{ls} + L_A & -\frac{1}{2}L_A & -\frac{1}{2}L_A \\ -\frac{1}{2}L_A & L_{ls} + L_A & -\frac{1}{2}L_A \\ -\frac{1}{2}L_A & -\frac{1}{2}L_A & L_{ls} + L_A \end{bmatrix}, \\ L_2(\theta_r) &= -L_B L(\theta_r), \end{aligned} \quad (11)$$

In (11), L_{sl} denotes the stator leakage inductance, L_A and L_B represent constant inductance terms, and $L(\theta_r)$ is defined by

$$L(\theta_r) = \begin{bmatrix} \cos(2\theta_r) & \cos(2\theta_r - \frac{2\pi}{3}) & \cos(2\theta_r + \frac{2\pi}{3}) \\ \cos(2\theta_r - \frac{2\pi}{3}) & \cos(2\theta_r + \frac{2\pi}{3}) & \cos(2\theta_r) \\ \cos(2\theta_r + \frac{2\pi}{3}) & \cos(2\theta_r) & \cos(2\theta_r - \frac{2\pi}{3}) \end{bmatrix}.$$

Substituting (10) into (9) yields

$$\begin{aligned} v_s^{abc} = (r_s I_3 + \omega_r \frac{d}{dt} L_2(\theta_r))i_s^{abc} + (L_1 + L_2(\theta_r))\frac{d}{dt} i_s^{abc} \\ + \lambda_m \omega_r \begin{bmatrix} \cos(\theta_r) \\ \cos(\theta_r - \frac{2\pi}{3}) \\ \cos(\theta_r + \frac{2\pi}{3}) \end{bmatrix}, \end{aligned} \quad (12)$$

which is a time-varying equation because θ_r changes over time. To render (12) time-invariant, we introduce *Park's transformation*

$$T(\theta) = \frac{2}{3} \begin{bmatrix} \cos(\theta) & \cos(\theta - \frac{2\pi}{3}) & \cos(\theta + \frac{2\pi}{3}) \\ \sin(\theta) & \sin(\theta - \frac{2\pi}{3}) & \sin(\theta + \frac{2\pi}{3}) \end{bmatrix}, \quad (13)$$

which converts variables in the *abc* reference frame to the *qd* reference frame (the zero component is omitted here); and the associated *inverse Park's transformation* is

$$T^{-1}(\theta) = \begin{bmatrix} \cos(\theta) & \sin(\theta) \\ \cos(\theta - \frac{2\pi}{3}) & \sin(\theta - \frac{2\pi}{3}) \\ \cos(\theta + \frac{2\pi}{3}) & \sin(\theta + \frac{2\pi}{3}) \end{bmatrix}, \quad (14)$$

where θ, any predefined rotation angle, is the argument of Park's transformation.

Applying Park's transformation and the inverse Park's transformation, the stator voltage, current, and flux linkage vectors in the *qd* and *abc* reference frames have the following relationships

$$\begin{aligned} v_s^{qd} &= T(\theta)v_s^{abc}, \quad v_s^{abc} = T^{-1}(\theta)v_s^{qd}, \\ i_s^{qd} &= T(\theta)i_s^{abc}, \quad i_s^{abc} = T^{-1}(\theta)i_s^{qd}, \\ \lambda_s^{qd} &= T(\theta)\lambda_s^{abc}, \quad \lambda_s^{abc} = T^{-1}(\theta)\lambda_s^{qd}. \end{aligned} \quad (15)$$

Now, given (13), (14), and (15), defining $\theta = \theta_r$, the dynamical equation of the PMSG (12) can be rewritten in the *qd* reference frame

$$v_s^{qd} = \begin{bmatrix} r_s & \omega_r L_d \\ -\omega_r L_q & r_s \end{bmatrix} i_s^{qd} + \begin{bmatrix} L_q & 0 \\ 0 & L_d \end{bmatrix} \frac{d}{dt} i_s^{qd} + \lambda_m \omega_r \begin{bmatrix} 1 \\ 0 \end{bmatrix}, \quad (16)$$

with

$$L_q = L_{sl} + \frac{3}{2}(L_A - L_B), \quad L_d = L_{sl} + \frac{3}{2}(L_A + L_B).$$

The stator current dynamics can be obtained by rearranging (16).

The generator torque. Let $\lambda_s^{qd} = [\lambda_{sq} \quad \lambda_{sd}]^\top$ and $i_s^{qd} = [i_{sq} \quad i_{sd}]^\top$, and then the generator torque in the *qd* reference frame is determined by

$$\Gamma_m = \frac{3}{2}\frac{\omega_r}{\omega_m}(\lambda_{sd} i_{sq} - \lambda_{sq} i_{sd}). \quad (17)$$

Using Park's transformation and its inverse transformation with $\theta = \theta_r$, the stator flux linkage (10) can be rewritten in the *qd* reference frame

$$\lambda_s^{qd} = \begin{bmatrix} L_q & 0 \\ 0 & L_d \end{bmatrix} i_s^{qd} + \lambda_m \begin{bmatrix} 0 \\ 1 \end{bmatrix}. \quad (18)$$

Substituting (18) into (17), the generator torque is obtained, namely,

$$\Gamma_m = \frac{3}{2} P(\lambda_m i_{sq} + (L_d - L_q) i_{sq} i_{sd}), \quad (19)$$

where $P = \frac{\omega_r}{\omega_m}$ denotes the number of pole pairs.

Equation (19) shows that the generator torque Γ_m is determined solely by the stator current i_s^{qd}, which facilitates the control of Γ_m by imposing controls on i_s^{qd}.

2.3 Generator Vector Control

The goal of the generator control is to drive the generator torque Γ_m and the reactive power of the generator stator Q_s to the desired values. Due to the facts that Γ_m and Q_s are difficult to measure; and there are relationships between reference values Γ_m^*, Q_s^*, i_{sq}^*, and i_{sd}^*, *i.e.*,

$$i_{sq}^* = \frac{2}{3P}\frac{\Gamma_m^*}{\lambda_m}, \quad i_{sd}^* = \frac{2}{3P}\frac{Q_s^*}{\omega_m \lambda_m}, \quad (20)$$

the goal of the generator control is achieved indirectly through the stator current feedback control.

We note that in (16) the q and d variables are coupled. To this end, the following feedback decoupling loop is considered.

$$v_s^{qd} = \hat{v}_s^{qd} + \begin{bmatrix} 0 & \omega_r L_d \\ -\omega_r L_q & 0 \end{bmatrix} i_s^{qd} + \lambda_m \omega_r \begin{bmatrix} 1 \\ 0 \end{bmatrix}. \quad (21)$$

where $\hat{v}_s^{qd} = [\hat{v}_{sq}, \hat{v}_{sd}]^{\mathrm{T}}$ is a vector of outputs of the current controllers. Assuming the decoupling is perfect, then the generator dynamics can be rewritten as

$$\hat{v}_s^{qd} = \begin{bmatrix} r_s & 0 \\ 0 & r_s \end{bmatrix} i_s^{qd} + \begin{bmatrix} L_q & 0 \\ 0 & L_d \end{bmatrix} \frac{d}{dt} i_s^{qd}. \quad (22)$$

Now, these equations can be split as two decoupled systems for q and d. Applying the Laplace transform to the above equations results in

$$\frac{i_{sq}}{\hat{v}_{sq}}(s) = \frac{1}{L_q s + r_s}, \qquad \frac{i_{sd}}{\hat{v}_{sd}}(s) = \frac{1}{L_d s + r_s}. \quad (23)$$

Finally, the stator currents i_{sq} and i_{sd} can be controlled separately by two PI controllers, namely

$$\hat{v}_{sq} = \frac{K_{pq} s + K_{iq}}{s}(i_{sq}^* - i_{sq}), \ \hat{v}_{sd} = \frac{K_{pd} s + K_{id}}{s}(i_{sd}^* - i_{sd}), \quad (24)$$

where K_{pq}, K_{iq}, K_{pd} and K_{id} are corresponding gains of the PI controllers.

2.4 Power Converter

The wind turbine generator is commonly connected to the power grid through a back-to-back converter. The back-to-back converter is an AC-DC-AC converter composed of a generator-side inverter, a grid-side inverter, and a DC bus in between. The DC bus contains a large capacitor in parallel which can be expressed as

$$\frac{d}{dt}V_{DC} = \frac{1}{C}i_{DC}, \quad i_{DCm} = i_{DC} + i_{DCl}, \tag{25}$$

where V_{DC} represents the DC bus voltage, C denotes the DC bus capacity, i_{DC} represents the current going through the DC bus capacity, i_{DCm} denotes the current coming from the generator-side inverter, and i_{DCl} denotes the current going through the gird-side inverter.

If two inverters are considered to be ideal without any losses, then the relationship between the AC-side and DC-side can be expressed as

$$\begin{aligned} \{v_l^{abc}\}^{\mathrm{T}} i_l^{abc} &= V_{DC} i_{DCl}, \\ \{v_s^{abc}\}^{\mathrm{T}} i_s^{abc} &= -V_{DC} i_{DCm}. \end{aligned} \tag{26}$$

where v_l^{abc}, i_l^{abc}, v_s^{abc} and i_s^{abc} are the grid-side voltage and current, and the generator-side voltage and current, respectively.

2.5 Grid Side Dynamics

Now we study the connection of the three-phase converter to the grid. If the three phases are considered to be balanced [5], then we have

$$v_l^{abc} = r_l i_l^{abc} + L_l \frac{d}{dt} i_l^{abc} + v_z^{abc}, \tag{27}$$

where v_l is the voltage between the inverter and DC bus neutral, v_z is the voltage between the transformer and its neutral, i_l is the current flowing through the converter, r_l is the grid connection resistance and L_l is the grid connection inductance.

We again simplify the equation (27) by Park transformation, namely

$$v_l^{qd} = r_l i_l^{qd} + L_l \frac{d}{dt} i_l^{qd} + L_l i_l^{qd} \dot{\theta} [T(\theta) \frac{d}{d\theta} T^{-1}(\theta)] + v_z^{qd}. \tag{28}$$

Note that the above equation can be further simplified. Recall the Park transformation (13) and inverse Park transformation (14), then we have the property such that

$$T(\theta) \frac{d}{d\theta} T^{-1}(\theta) = \begin{bmatrix} 0 & 1 \\ -1 & 0 \end{bmatrix}. \tag{29}$$

Substitute (29) in (28) yields the grid side dynamics

$$v_l^{qd} = \begin{bmatrix} r_l & L_l \dot{\theta} \\ -L_l \dot{\theta} & r_l \end{bmatrix} i_l^{qd} + L_l \frac{d}{dt} i_l^{qd} + v_z^{qd}. \tag{30}$$

2.6 Grid Side Control

DC bus voltage regulation. The DC bus dynamics is described by (25). Applying the Laplace transformation to this equation yields

$$V_{DC}(s) = \frac{1}{Cs} i_{DCm}(s) - \frac{1}{Cs} i_{DCl}(s) \tag{31}$$

[5] For an unbalanced grid, a similar equation can be obtained by applying the variable change based on the homopolar sequence of v_l and v_z.

To control the DC bus voltage, we consider a simple PI controller, namely

$$K(s) = \frac{K_{pg} s + K_{ig}}{s} \tag{32}$$

where K_{pg} and K_{ig} are the proportion and integral gains, respectively. This leads to the closed-loop transfer function

$$T(s) = \frac{V_{DC}}{V_{DC}^*} = \frac{\frac{K(s)}{Cs}}{1 + \frac{K(s)}{Cs}}, \tag{33}$$

where V_{DC}^* is the reference value of the DC bus voltage.

If the current control loop ensures an ideal instantaneous response (*i.e.* $i_{DCl} = i_{DCl}^*$), then the current reference i_{DCl}^* can be expressed as

$$i_{DCl}^* = K(s)(V_{DC}^* - V_{DC}) + i_{DCm}. \tag{34}$$

AC side current control. Similar to the generator vector control, the AC side current is controlled by a feedback loop comparing the desired and actual current. Again, we calculate the current reference from the power reference as

$$i_{lq}^* = \frac{2}{3} \frac{P_z^*}{v_{zq}} = \frac{2}{3} \frac{V_{DC}}{v_{zq}} i_{DCl}^*, \quad i_{ld}^* = \frac{2}{3} \frac{Q_z^*}{v_{zq}} = 0, \tag{35}$$

where i_{lq}^* and i_{ld}^* are the calculated current reference values. P_z^* and Q_z^* are the power reference values at the grid connection point. Recall (30) with θ such that the q-axis is aligned with the voltage and the d-axis leads the q-axis, *i.e.* $v_{zd} = 0$ and $\dot{\theta} = 2\pi f$. There is a coupling between the q and d variables. Again, we apply the similar decoupling method as in Section 2.3, considering a feedback decoupling loop as follows.

$$v_l^{qd} = \hat{v}_l^{qd} + \begin{bmatrix} 0 & 2\pi f L_l \\ -2\pi f L_l & 0 \end{bmatrix} i_l^{qd} + \begin{bmatrix} v_{zq} \\ 0 \end{bmatrix} \tag{36}$$

where f is the electrical network frequency, $\hat{v}_l^{qd} = [\hat{v}_{lq} \quad \hat{v}_{ld}]^{\mathrm{T}}$ represents the outputs of the current controllers. Assuming the decoupling is perfect, then the dynamics of the system become

$$\hat{v}_l^{qd} = \begin{bmatrix} r_l & 0 \\ 0 & r_l \end{bmatrix} i_l^{qd} + \begin{bmatrix} L_l & 0 \\ 0 & L_l \end{bmatrix} \frac{d}{dt} i_l^{qd}. \tag{37}$$

Then, the current i_l^{qd} can be controlled by two independent PI controllers, namely

$$\hat{v}_{lq} = \frac{K_{pc} s + K_{ic}}{s} (i_{lq}^* - i_{lq}), \ \hat{v}_{ld} = \frac{K_{pc} s + K_{ic}}{s} (i_{ld}^* - i_{ld}), \tag{38}$$

where K_{pc} and K_{ic} are the corresponding gains of the PI controllers.

3. WIND FARM MODEL

In this section, the schematic outline of the wind farm is presented. A $N_s \times 1$ MW wind farm on a 66 kV distribution feeder is created, as shown in Fig. 1, where N_s denotes the number of strings. In Fig. 1, each triangle represents a wind turbine generator described in Section 2 (see Fig. 2). The wind farm of interest comprises N_s strings of wind turbines. On each string, there are 10 generators, each of which is attached to a transformer. These generators with transformers are then connected to each other through cable lines with capacitors in parallel.

The mathematical description of an ideal transformer is represented by

$$v_1^{qd} - v_W^{qd} = \begin{bmatrix} R_T & L_T\dot{\theta} \\ -L_T\dot{\theta} & R_T \end{bmatrix} i_1^{qd} + L_T \frac{d}{dt} i_1^{qd}, \quad v_W^{qd} = K v_N^{qd},$$
$$v_N^{qd} - v_2^{qd} = \begin{bmatrix} R_Z & L_Z\dot{\theta} \\ -L_Z\dot{\theta} & R_Z \end{bmatrix} i_2^{qd} + L_Z \frac{d}{dt} i_2^{qd}, \quad i_2^{qd} = K i_1^{qd}, \tag{39}$$

where K is the turns ratio of the transformer, v_W^{qd} and v_N^{qd} are the generator-side and grid-side neutral point voltage, v_1^{qd}, i_1^{qd}, R_T and L_T are the generator-side voltage, current, resistance and inductance and v_2^{qd}, i_2^{qd}, R_Z and L_Z are the grid-side voltage, current, resistance and inductance. The dynamics of the cable lines and of the capacitors are described as

$$\frac{d}{dt} v_c^{qd} = \begin{bmatrix} 0 & -\dot{\theta} \\ \dot{\theta} & 0 \end{bmatrix} v_c^{qd} + \frac{1}{C} i_c^{qd},$$
$$\frac{d}{dt} i_{line}^{qd} = \frac{1}{L} \begin{bmatrix} -R & -L\dot{\theta} \\ L\dot{\theta} & -R \end{bmatrix} i_{line}^{qd} + v_{line}^{qd}, \tag{40}$$

where C denotes the capacitance, R denotes the cable line resistance, and L denotes the cable line inductance; v_c^{qd}, i_c^{qd}, v_{line}^{qd}, and i_{line}^{qd} are the corresponding voltages and currents, respectively. Finally, the model of a string is obtained by considering (39), (40), and the equations in Fig. 2.

As shown in Fig. 1, the N_s strings are coupled through a wind farm transformer whose feeder side is denoted as the point of common coupling (PCC), assuming that other loads or generators may be connected to the point in real-world scenarios. The dynamical model of each wind turbine generator, including the impedance [6] on the generator side, is of dimension 17.

The entire wind farm is modelled using Matlab/Simulink and a complete example of this benchmark can be downloaded from Zhang et al. (2024). Although the wake effect is not modelled in this section, it can be easily implemented in the provided Simulink model by assigning specific wind speed values for each wind turbine. The order of the proposed model is $(N_s \times 10 \times 17 + 4)$, which shows the possibility that MOR methods can be validated on different scales by tuning the number of strings. The input and output of the system can be selected as the root mean square (rms) value of the PCC voltage and the active power of the wind farm, respectively, for testing MOR on single-input single-output (SISO) systems; or can be selected as the PCC voltage vector in the qd reference frame, and the active and reactive power of the wind farm, respectively, for testing MOR on multi-input multi-output (MIMO) systems.

4. NUMERICAL EXAMPLES

In this section, we use the SISO wind farm model described in Section 3 with $N_s = 2$ (thus, the order is 344) as a benchmark model to show the performance of different types of MOR techniques. Because of space constraints, we mainly deliver the simulation results. Readers are referred to the provided references in the following subsections for the details of the MOR methods and Zhang et al. (2024) for the details of the implementation of these MOR methods.

[6] The impedance on the generator side includes the resistance of the cable line, the capacitor, and the wind turbine generator transformer, which are represented by short and red lines in Fig. 1.

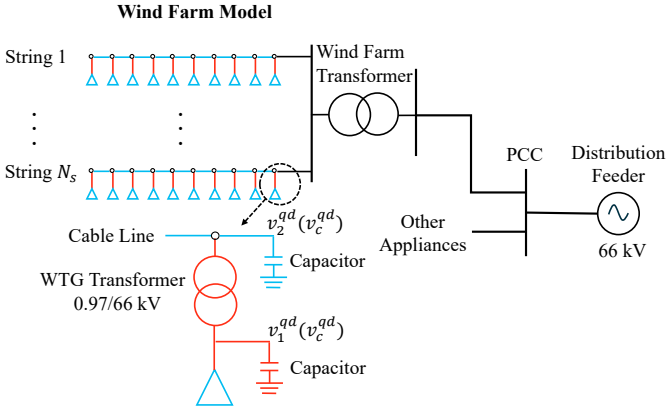

Fig. 1. The schematic outline of the wind farm.

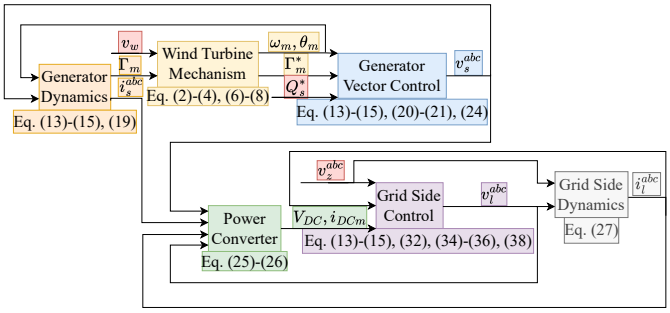

Fig. 2. The outline of the wind turbine generator.

4.1 MOR for Nonlinear Systems

In this section, the wind farm model is utilised to show the effectiveness of a data-driven nonlinear MOR method proposed in Scarciotti and Astolfi (2017). The method is tested using constant wind speed 7.5; the data is generated using a linear signal generator composed of frequencies $f_1 = 1.157 \times 10^{-5}$ Hz, $f_2 = 0.025$ Hz, $f_3 = 0.143$ Hz, $f_4 = 0.11$ Hz, and $f_5 = 0.2$ Hz; the approximate moment is calculated by 20 radius basis functions (RBFs). With these settings, a reduced-order model of order 11 is obtained and its performance is shown in Fig. 3. The top graph depicts the output responses of the full-order model (FOM) (solid/blue line) and of the reduced-order model (ROM) (dashed/red line). The bottom graph depicts their corresponding absolute error. This simulation shows that the proposed wind farm model can be effectively used for testing nonlinear MOR methods.

4.2 MOR for Linear Systems

In this section, the wind farm model is linearised [7] at $t = 40$ s, and then the linearized model is reduced using the two-sided moment matching method Ionescu (2015). Using this method, we obtain a reduced-order model of order 20, which matches the moments of the linearised wind

[7] Using the *linearize* function in Matlab at a specific time snapshot.

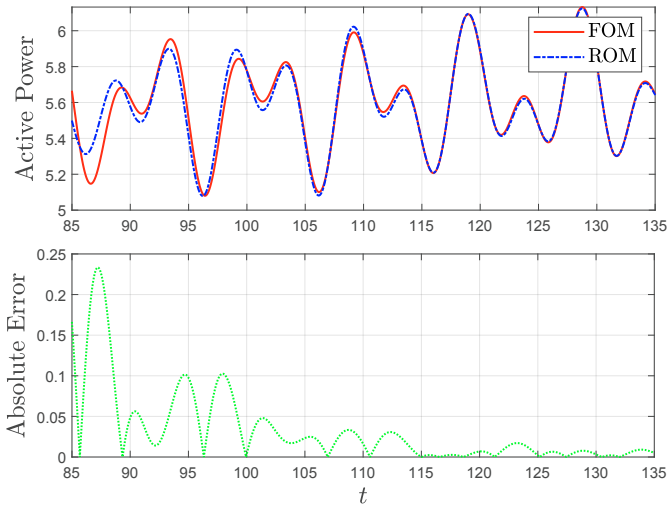

Fig. 3. Top graph: time histories of the output response of the full-order model (solid/blue line) and of the output response of the obtained reduced-order model (solid/red line). Bottom graph: the absolute error between the output of the FOM and that of the ROM.

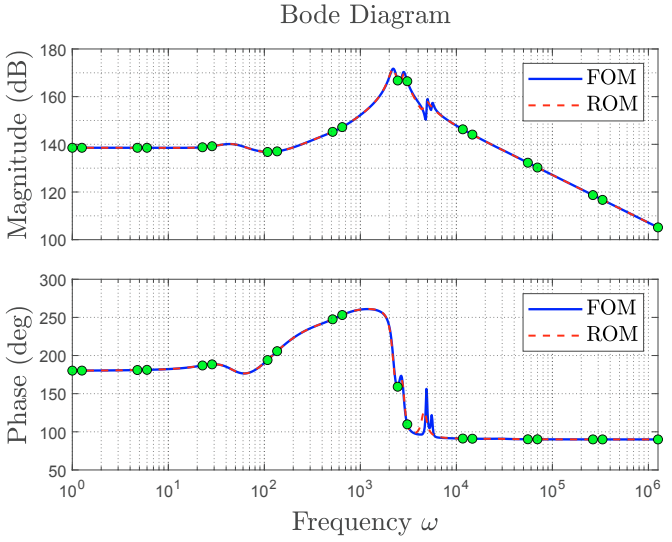

Fig. 4. Frequency responses of the FOM (solid/blue line) and of the ROM (dashed/red line). The green circles indicate the frequency interpolation points.

farm model at a set of predefined interpolation points. The frequency response of the full-order model (solid/blue line) and that of the reduced-order model (dashed/red line) are given in Fig. 4. The green circles indicate the frequency interpolation points which are sampled logarithmically from 10^0 to 10^6 rad/s. Fig. 4 shows that the linearised wind farm model can be used as a benchmark model for testing linear MOR methods.

REFERENCES

Ali, H.R., Kunjumuhammed, L.P., Pal, B.C., Adamczyk, A.G., and Vershinin, K. (2018). Model order reduction of wind farms: Linear approach. *IEEE Transactions on Sustainable Energy*, 10(3), 1194–1205.

Antoulas, A.C. (2005). *Approximation of large-scale dynamical systems*. SIAM.

Astolfi, A. (2010). Model reduction by moment matching for linear and nonlinear systems. *IEEE Transactions on Automatic Control*, 55(10), 2321–2336.

Besselink, B., van de Wouw, N., Scherpen, J.M., and Nijmeijer, H. (2014). Model reduction for nonlinear systems by incremental balanced truncation. *IEEE Transactions on Automatic Control*, 59(10), 2739–2753.

Bond, B.N. and Daniel, L. (2007). A piecewise-linear moment-matching approach to parameterized model-order reduction for highly nonlinear systems. *IEEE Transactions on Computer-Aided Design of Integrated Circuits and Systems*, 26(12), 2116–2129.

Fujimoto, K. and Scherpen, J.M. (2010). Balanced realization and model order reduction for nonlinear systems based on singular value analysis. *SIAM Journal on Control and Optimization*, 48(7), 4591–4623.

Gong, Z., Mao, J., Junyent-Ferré, A., and Scarciotti, G. (2024). Model order reduction of large-scale wind farms: A data-driven approach. *IEEE Transactions on Power Systems*.

Heier, S. (2014). *Grid integration of wind energy: onshore and offshore conversion systems*. John Wiley & Sons.

Ionescu, T.C. (2015). Two-sided time-domain moment matching for linear systems. *IEEE Transactions on Automatic Control*, 61(9), 2632–2637.

Janssen, L.A., Besselink, B., Fey, R.H., and van de Wouw, N. (2024). Modular model reduction of interconnected systems: A robust performance analysis perspective. *Automatica*, 160, 111423.

Junyent Ferré, A. (2011). Control of power electronic converters for the operation of wind generation. *PhD Thesis*.

Kawano, Y. and Scherpen, J.M. (2021). Empirical differential gramians for nonlinear model reduction. *Automatica*, 127, 109534.

Leidhold, R., Garcia, G., and Valla, M. (2002). Maximum efficiency control for variable speed wind driven generators with speed and power limits. In *IEEE 2002 28th Annual Conference of the Industrial Electronics Society. IECON 02*, volume 1, 157–162. IEEE.

Rafiq, D. and Bazaz, M.A. (2023). A collection of large-scale benchmark models for nonlinear model order reduction. *Archives of Computational Methods in Engineering*, 30, 69–83.

Scarciotti, G. (2016). Low computational complexity model reduction of power systems with preservation of physical characteristics. *IEEE Transactions on Power Systems*, 32(1), 743–752.

Scarciotti, G. and Astolfi, A. (2017). Data-driven model reduction by moment matching for linear and nonlinear systems. *Automatica*, 79, 340–351.

Scarciotti, G. and Astolfi, A. (2024). Interconnection-based model order reduction-a survey. *European Journal of Control*, 75, 100929.

Simard, J.D. and Astolfi, A. (2021). Nonlinear model reduction in the loewner framework. *IEEE Transactions on Automatic Control*, 66(12), 5711–5726.

The MORwiki Community (N.D.). MORwiki - Model Order Reduction Wiki. `http://modelreduction.org`.

Zhang, H., Gong, Z., Junyent-Ferré, A., and Scarciotti, G. (2024). Wind_Farm_A_Benchmark_Model_for_MOR. `https://github.com/hz1021/Wind_Farm_A_Benchmark_Model_for_MOR`.